International Journal of Precision Engineering and Manufacturing-Green Technology
https://doi.org/10.1007/s40684-020-00282-8

Online ISSN 2198-0810
Print ISSN 2288-6206

REGULAR PAPER

Biomimetic Flow Sensor for Detecting Flow Rate and Direction as an Application for Maneuvering Autonomous Underwater Vehicle

Le-Giang Tran[1] · **Woo-Tae Park**[1,2]

Received: 28 February 2020 / Revised: 19 October 2020 / Accepted: 26 October 2020

Abstract

Attaining the information of the hydrodynamic flow rate and direction is essential to the maneuvering of autonomous underwater vehicles (AUVs). This work presents a pillar-based flow sensor that measures hydrodynamic flow rate and direction. We propose a design that mimic the working principle of the neuromast, a ubiquitous organ in fishes that sense the water flow. By utilizing advances in piezo-resistive pressure sensors and 3D printing technology, sensor fabrication becomes fast and cost-effective, owing to reductions in labor and material cost for small batches. Measured results showed that the sensor sensitivity was 9.24 mV/m/s in the single mode and 20.3 mV/m/s in the differential mode. The resolution of the flow sensor was measured to be 4.93 mm/s in the water tunnel testing. The angular resolution of the flow sensor was 2.25°.

Keywords Flow sensors · Autonomous underwater vehicles (AUVs) · Neuromast · Pillar-based sensor · Pressure sensor · Piezoresistive sensor

List of Symbols

A_{drag}	The cupula area subjected to the flow
A_c	The contact area
C_D	Drag coefficient
F_{drag}	The drag force applied to the cupula
F_{push}	The moment delivered to the Ecoflex™ layer
h	The length from the cupula center of mass to the cilia's center of rotation
P	Pressure
u	Flow rate
V_{out}	Output voltage
w	The length of the cilia leg
ρ	Liquid density
δ	Sensitivity
β	Offset

1 Introduction

Roughly 70% of the Earth's surface is covered with water [1]. Work in many research areas is driving further discoveries of the underwater environment and explorations of its geography. Since safety, efficiency and operation cost were priorities in the marine environment and geoscience researches, the demand for functional robots to take over humans in the examination of the ocean floor has been emerging. Development of AUVs technology can facilitate actions to save the marine environment from adverse human activities.

This prompted the development of autonomous underwater vehicles (AUVs) to support the discovery process [2]. The history of AUVs began in the 1970s but the technical issue of navigation and localization remains challenging to present days [3]. A variety of technologies was utilized to control AUVs. Controlling AUVs requires integration of multiples sensor system such as global positioning system (GPS), Doppler velocity log (DVL) and inertial measurement unit (IMU) [4, 4]. Along with indirect navigation and inertial measurement approaches, measuring relative hydrodynamic flow around AUVs also provides crucial data for AUV maneuvering.

The process of evolution has equipped creatures with unique solutions for specific functions, which can all be studied for the purposes of biomimicry. The efficiency,

✉ Woo-Tae Park
wtpark@seoultech.ac.kr

[1] Convergence Institute of Biomedical Engineering and Biomaterials, Seoul National University of Science and Technology, Seoul 01811, Korea

[2] Department of Mechanical Engineering, Seoul National University of Science and Technology, Seoul, Korea

Published online: 30 November 2020

reliability and precision of nature's design is the ultimate goals that inspired the design of this artificial pillar-based flow sensor. For example, the blind cavefish, which spends its entire life in the deep and dark water zone, has developed a set of highly sensitive neuromasts that can sense steady flow rate down to 10 mm/s [6] and 18–35 μm/s for 10–20 Hz oscillation flow [7]. These exceptionally large neuromasts provide the blind cavefish with higher sensitivity than other fish [8]. In nature, the neuromasts and lateral line system evolved to attain a distinctive sense generally called "hydrodynamic vision" [9]. By integrating information of hydrodynamic flow and pressure, fish are able to effectively regulate their swimming, schooling, hunting and hiding activities [10].

From the engineering perspective, hydrodynamic flow is comprised of three components: velocity, frequency, and direction. There are various mechanisms which can be used to measure the hydrodynamic flow rate including pressure sensors [11, 12], optical reflection [13, 14], piezoelectric and piezoresistive effects [15–17] and thermal transfer [18, 19]. In terms of design, some works found inspiration in the cricket's filiform hairs [20–22] while other works attempted to mimic the canal neuromast sensor found in fish [23, 24]. These approaches possess unique attributes in terms of sensitivity, resolution, and the capability to detect flow direction.

The advance of micromachining technology makes it possible to study and imitate the biological structures and mechanisms [25]. Many works have attempted to mimic fish's neuromast and lateral line for flow sensing. Fan et al. developed a vertical PDMS cilium attached to a piezoresistive cantilever [26]. In that work, when fluid flow was applied to the cilium, force was transferred to the cantilever, causing resistive change. Mathematical and experimental results have confirmed that the change in resistance was proportional to the square of the flow velocity. Ko et al. proposed a piezoresistive acceleration sensor that mimicked filiform hairs by attaching a rigid rod to the top of a piezoresistive membrane [27]. The piezoelectric effect is another solution for flow sensing that offers the benefit of self-generated power. Bian et al. coated a metal core cilium with a piezoelectric ceramic to mimic the working principle of the cricket's filiform hairs [20]. When the cilium was bent and deformed, repolarization occurred in the piezoelectric ceramic electrode, thus inducing a voltage between two electrodes. The cilium structure was successfully mimicked to sense flow rate in previous works [28]. Furthermore, flow direction can be detected if multiple flow sensors are integrated in four cardinal directions. This principle is applicable for a variety of sensing mechanism such as piezoresistance [29, 30], optical reflection [13] or thermal transfer [31]. Xu et al. proposed a setup of multiple pressure sensors along an autonomous underwater vehicle which detects obstacles by comparing the magnitude and phase difference in each sensor [32].

The majority of the previous designs for flow sensing involve adhering a cilia structure to the top of either a piezoresistive or a piezoelectric membrane. Modifications to the flow cilia structure provide different characteristics to the sensor. This simple solution has proven itself practically in terms of efficiency, reliability, and accuracy. It is, however, omnidirectional, in that the sensor provides the same output for flows from any direction. It is this limitation that restricts the maneuvering of AUVs in a practical situation.

In this work, we aimed to sense flow rate and flow direction simultaneously by mimicking the morphology of the neuromast among fishes (Fig. 1). Unlike highly sensitive flow sensors used for object detection [33, 34] our pillar-based flow sensor was expected to encounter strong flow currents in its environment. Thus, achieving a consistently robust design was desirable. Advanced 3D printing technology was applied to fabricate the complex cilia. Multiple pressure sensors were then integrated into the novel cilium mimicking unit. As a result, both flow velocity and direction were obtained from a single flow sensor. The developed flow sensor is expected to improve the maneuvering of AUVs for self-exploration applications.

2 Methods

2.1 Sensing Principle

The lateral line in fish performs a critical role in the fish's perception including schooling, detecting reverse flow, and avoiding obstacles [35]. The lateral line consists of

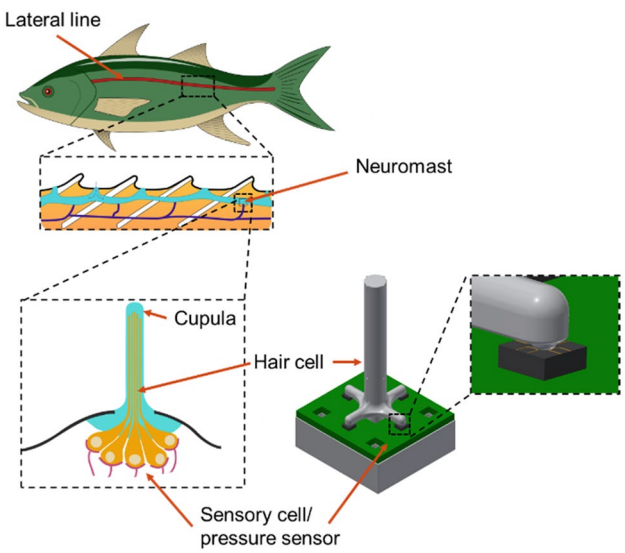

Fig. 1 The concept of the biomimetic flow sensor

neuromast units, which are composed of a staircase group of sensory hair cells, covered by a cupula, an elastic structure that deforms to the water flow, and connected to the nerves [36]. The natural designs of the hair cell are diverse. The cupula is either exposed to the external flow (superficial neuromasts or SNs) or enclosed inside the lateral channel (canal neuromasts or CNs) [37]. In both cases, water flow deforms the cupula. The sensory hair detects these changes and sends the signal to the nerves through sensory cells.

The flow rate sensor discussed in this work is comprised of four off-the-shelf piezoresistive pressure sensors, a printed circuit board, a biomimetic pillar structure and a PDMS cupula (Fig. 3). The artificial pillar was inspired by the structure of a fish hair cell.

The flow sensor was designed to apply the same sensing principle as the neuromast. The 3D-printed pillar resembles a natural sensory hair cell, and the pressure sensors serve the same purpose as the sensory cells.

For the sensing element, a gauge type die-level pressure sensor (SM30D, Silicon Microstructures, Inc, Milpitas, CA, USA) was utilized. This pressure sensor die was gauge type where the reference pressure was taken as atmospheric pressure (open to air). The sensor was designed to be operated within a pressure range of 0–80 PSI with a standard supply voltage of 5 V.

In order to detect flow direction, four pressure sensor dies were integrated into a single PCB following four cardinal directions. The arrangement of the pressure sensor dies and pillar is depicted in a top-down view in Fig. 2b. As the amplitude of the output voltage scales with the flow rate, flow direction can be detected by comparing the output amplitude of the four pressure sensors. For example, with horizontal flow (from left to right), the pillar will tilt to the right in accordance with the lever principle (Fig. 2b). It will thus transmit the drag force it received to a push on sensor 3 and a pull at sensor 1 while delivering no actuation on sensor 2 and 4.

The pressure sensors' output signal readout was collected by a data acquisition device (DAQ). Analysis of the frequency spectrum and low pass filter was processed on MATLAB program.

2.2 Theoretical Model

We have deduced a model that relates the Wheatstone bridge output voltage to the fluid flow rate. We calculated the drag force generated by the flow and convert this force to the pressured applied on the pressure sensor. This relation was described by a second order equation, which is referred as the general equation.

The drag force applied on the cupula is a function of flow rate u, drag coefficient C_D, subjected area A_{drag} and liquid density ρ.

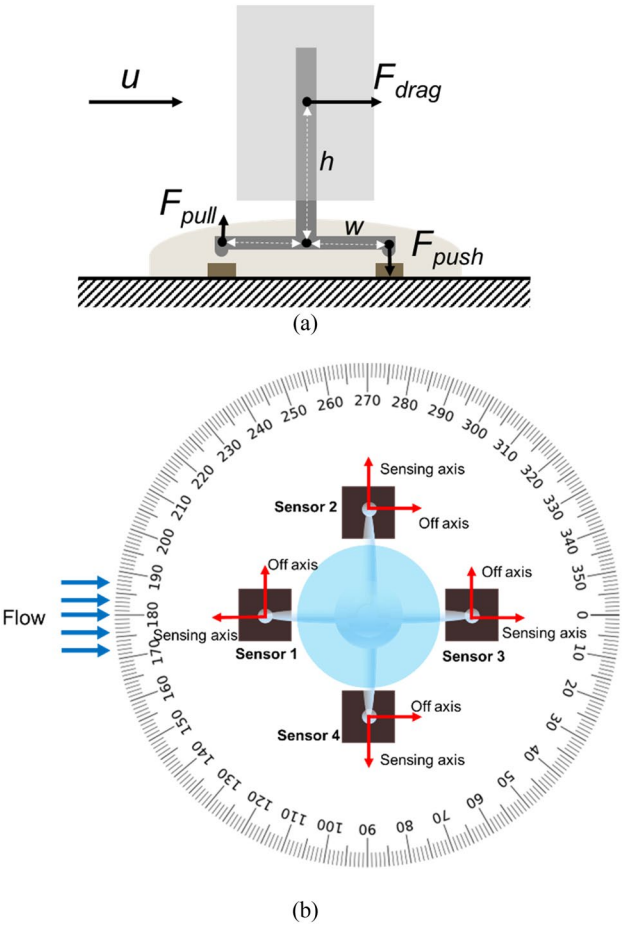

Fig. 2 Sensing mechanism of the flow sensor. **a** The drag force interaction model of the pillar. **b** Top view of the arrangement of the four pressure sensors under the artificial pillar allowing directional sensing of the flow

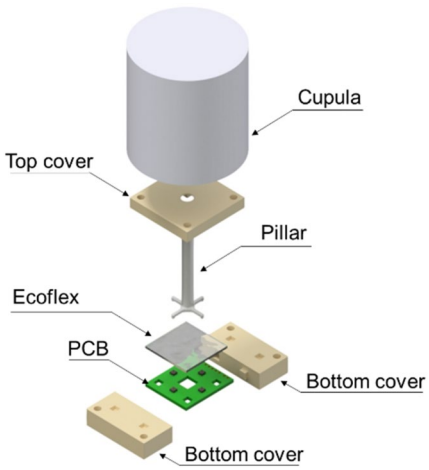

Fig. 3 Flow sensor assembly

$$F_{drag} = \frac{1}{2} C_D \rho u^2 A_{drag} \tag{1}$$

We considered the PDMS cupula and pillar structure forms a united structure. Then, the moment F_{push} that delivered to the Ecoflex™ layer and pressure sensor is considered as following:

$$F_{push} = \frac{h}{w} F_{drag} \tag{2}$$

where h, w is the length of the links.

By assuming the contact area A_c, the moment applied on the pressure sensor was converted to pressure:

$$P = \frac{F_{push}}{A_c} \tag{3}$$

Owing to the linearity of the pressure sensor die, the output voltage of the sensor was calculated using the sensitivity δ and offset β:

$$V_{out} = \delta P + \beta \tag{4}$$

Integrating Eqs. (1), (2), (3) and (4), we obtained the general function relating the flow rate and flow sensor's output voltage:

$$V_{out} = \frac{h\delta C_D \rho u^2 A_{drag}}{2wA_c} + \beta \tag{5}$$

The general Eq. (5) confirmed that the output voltage V_{out} is proportional to the second order of the flow rate u.

In this model, the effect of cupula size on sensor performance can be deduced from Eq. (5). For example, if the radius of the cylinder is doubled, the subjected area A_{drag} is quadrupled, therefore, the V_{out} is also quadrupled. Equation (5) also implies a trade-off between sensor performance and size.

2.3 Fabrication

The flow sensor assembly diagram is shown in Fig. 3. Firstly, 3 g of Ecoflex™ 0050 was poured to a 5 cm Petri dish containing the PCB to form a thin layer of Ecoflex™ on top of the pressure sensor. Secondly, the pillar was carefully aligned with the four legs resting precisely on four pressure sensor dies. An additional amount of Ecoflex™ was poured on the pillar legs to cover and affix the pillar position. Then, the bottom and top 3D printed covers were attached. The PDMS cupula, which was replicated from a 3D printed mold, was then attached to the cilia. Electrical connectors were soldered to the PCB to complete the assembly process. Lastly, Sil-Poxy silicon rubber adhesive (Smooth-On Inc, USA) was used to seal all exposed electrical connections for water-proofing.

2.4 Calibration

The equipment setup for the calibration experiment is shown in Fig. 4a. The goal of this experiment was to calibrate the flow sensor so that a linear correlation could be verified between a known applied force on the pillar and the output voltage of the flow sensor. In the setup, the load cell, a transducer used to measure compressive force, was attached to a programmable stage. A small range load cell (SMN-2L, CAS, S. Korea) was used in this experiment. The stage was set to move vertically at a velocity of

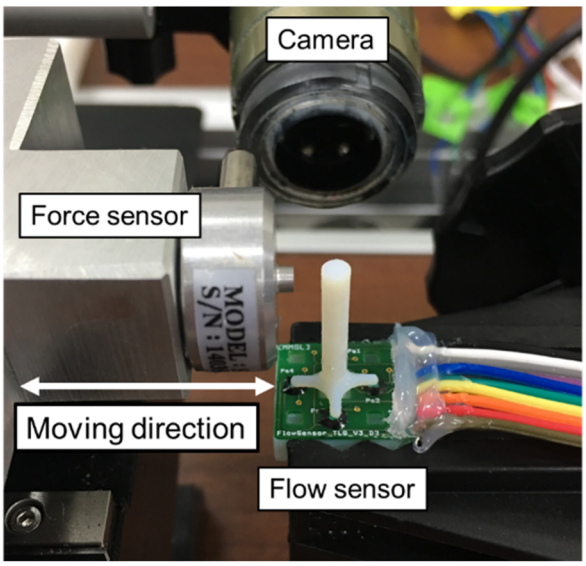

(a)

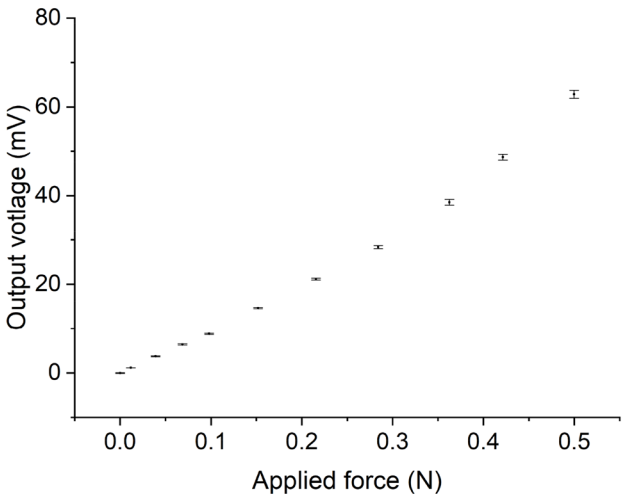

(b)

Fig. 4 **a** Setup of the calibration test showing the load cell. **b** The output voltage versus applied force of the flow sensor

0.01 mm/s. The movement was controlled via a computer. The load cell was moved forward to exert a certain level of force on the pillar which was held for 30 s. The micro controller interface recorded data during this 30 s period, after that the load cell was moved again to increase the applied force to the next level displacement for another 30 s. A USB camera (Dino LITE, AM4113T) was arranged to focus on the cilia, allowing the observer to examine the experiment process. A micro controller was utilized to collect the flow sensor's output in this experiment.

2.5 Water Tunnel Test

The second experiment examined the performance of the sensor in a water tunnel. The water flow was generated and controlled by a pump. A continuous circulating flow was introduced into a square acrylic tunnel (Fig. 5). This setup was advantageous for low flow rate as relatively laminar flow was observed with flow velocity under 200 mm/s. The sensor was fixed to the bottom of the tunnel with adhesive tapes. To monitor the applied flow rate in the water tunnel, particle image velocimetry (PIV, particle image velocimetry) method was used. This method detects the velocity vectors with high accuracy and has high temporal resolution in fractions of a second [38]. Additionally, PIV allows measuring the flow field without interfering the flow, enabling us to find the precise flow rate that is applied to our flow sensor.

2.6 Angular Test

The angular resolution of the flow sensor was tested in air with a manual rotation base. In the angular testing experiment, we recorded the output voltage of the four pressure sensors while rotating the sensor from 0° to 360° at the increasement of 3°. Data acquisition system (MonoDAQ-U-X) was implemented to record signals of four sensors simultaneously. Low pass filter and normalization was applied in this test for the convenience of comparison.

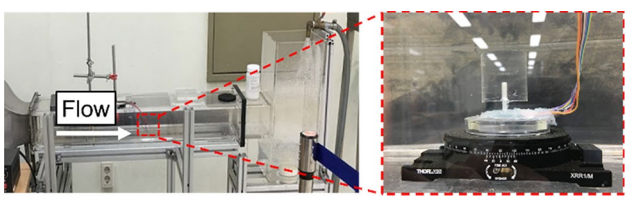

Fig. 5 The setup to measure the sensitivity of the flow sensor in the water tunnel. In this setup, water flows from left to right, in parallel with sensor 1 and 3

3 Experimental Results and Discussion

In the interest of characterizing the flow sensor, three principal experiments were conducted. The first experiment investigated the sensitivity of the sensor's output. In the second experiment, the performance of the flow sensor underwater was tested for different flow velocities. Finally, in the third experiment, the angular resolution was examined.

3.1 Sensor Calibration

The calibration result was plotted in Fig. 4b. The load cell exerted a force ranging from 0 to 0.54 N on the pressure sensor and induced a corresponding output voltage ranging from 0 to 78 mV. A linear fit model was proposed for the graph with an R-square value of 98%. In this paper, we considered the R-squared larger than 90% indicated a good linear regression to the data. The slope of the fit line, which is the force sensitivity was measured to be 131.6 mV/N.

3.2 Water Tunnel Experiment

In this experiment, signal of a single pressure sensor was processed to detect the flow rate. Figure 6 showed response of the flow sensor to different conditions of flow rate. First, the relation between the sensor 3 output voltage and the flow rate was quadratic, which is in agreement with the general Eq. (5). Additionally, we observed that when the flow rate is less than 231 mm/s, the response of the flow sensor was quite linear. Therefore, a linear fit model was

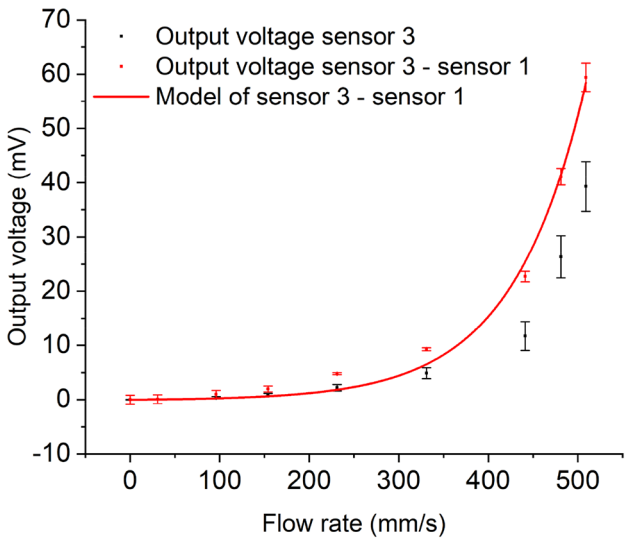

Fig. 6 The exponential response in single mode (sensor 3) and differential mode (sensor 3–sensor 1) to the water flow rate. The model of the differential mode was calculated based empirical model in Eq. (6)

applied to the output voltage at the flow rate ranging from 0 to 231 mm/s with the R-square of 90.5%. Therefore, the linear sensitivity of sensor 3 in the low flow rate was calculated to be 9.24 mV/m/s.

The noise and uncertainty of the flow sensor was investigated in order to determine the resolution of the sensor. Sources of noise were various, including the sensor's intrinsic noise, electronic noise in the data acquisition devices and environment, and the turbulence of the water or air flow. In order to measure the intrinsic noise of this sensor, we recorded the sensor's output voltage as it was excited by 5 V DC without the input flow stimulus. The average peak to peak voltage of this measurement was determined to be the intrinsic noise of the flow sensor, which was measured to be 0.084 mV maximum. This noise level was related to the minimum resolution of the flow sensor. The linear resolution in this case can be calculated by taking the ratio between the noise voltage and sensitivity, which was 6.93 mm/s in sensor 3.

By observation, it was noticed that the flow in the water tunnel was steady and laminar when the flow rate was less than 200 mm/s. At the onset of 200 mm/s and beyond, turbulence flow can be observed in the water tunnel. The strong turbulence at high flow rate explained the noise that was recorded as seen in Fig. 7. Additionally, it is noticed that during the experiment at the instant of changing water flow rate, there was a short period of 2–5 s that the flow had strong fluctuation, which was also reflected in Fig. 7.

It was observed that the two opposite sensors (for example, sensor 1 and 3) produced reverse output voltage (Fig. 7a). An explanation for this relation would be the effect of the Ecoflex™ coating. As the Ecoflex™ covered the pillar legs and pressure sensor membrane, when pillar leg pressed on the sensor 3, it also pulled the membrane of sensor 1 upward, resulting in a reverse response in sensor 1. In term of the amplitude, sensor 3 produced the output voltage larger than that of sensor 1 fivefold. Therefore, it is better to detect the flow rate by using the difference between the voltage of sensor 3 and sensor 1. Figure 7b showed the differential voltage of sensor 3 and sensor 1 versus the flow rate. Again, the linear fit was implemented for the flow rate less than 231 mm/s to find the linear flow rate sensitivity with the R-squared of 92.2%. In this case, the calculated sensitivity was 20.3 V/mm/s, which is also twice the low flow rate sensitivity of sensor 3 solely. The resolution of the differential mode was calculated to be 4.93 mm/s. Notice that the calculated linear sensitivity was valid for the low flow rate only. Furthermore, doubling the sensitivity also doubles the resolution. Therefore, the differential voltage of the two opposite sensors was preferable to detect the flow rate more accurately.

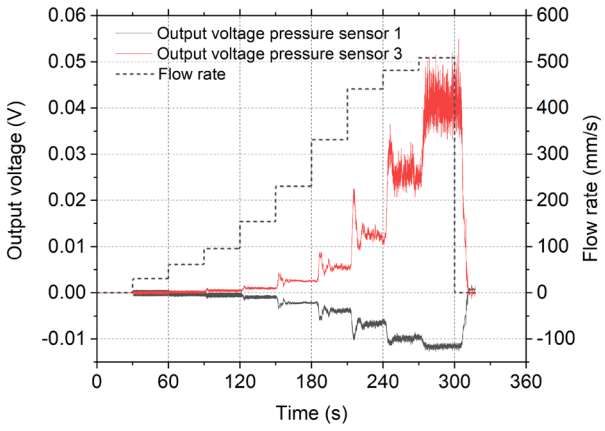

(a)

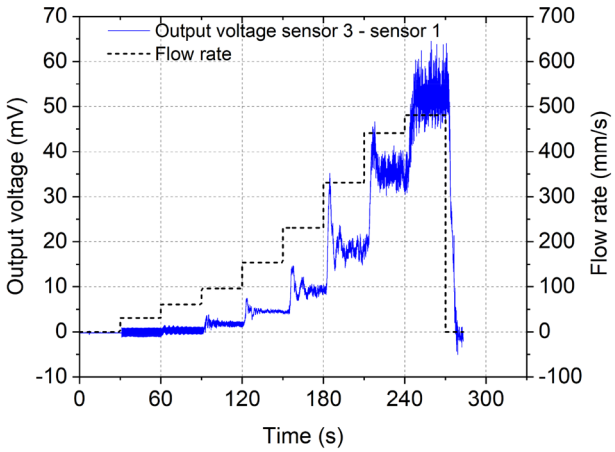

(b)

Fig. 7 The temporal response of the flow sensor in the water tunnel. **a** Comparison between the two opposite sensors 1 and 3. **b** The differential voltage of sensor 3 and sensor 1. The right-*y* axis in both graphs indicates the input flow rate as controlled by the pump in the water tunnel

An exponential equation was proposed for the differential voltage of sensor 3 and sensor 1 to associate input flow rate and output voltage in Fig. 6:

$$V_{out} = -0.116(1 - e^{-0.012u}) \tag{6}$$

where V_{out} is output voltage of the sensor measured in mV and u is flow rate in the water tunnel measured in mm/s. The exponential empirical model obtained an R-squared of 99% to measured data.

3.3 Directional Detection Experiment

When rotating the flow sensor for 360°, each part of the pressure sensors produced a sinusoidal signal proportional to the rotation angle. Output voltage of each pressure sensor was normalized. The plot of the normalized output of four pressure sensors showed a good fit to four sinusoidal waves (Fig. 10). We calculated the angular resolution based on the uncertainty of the output voltage. The tool to calculate the angular resolution was adapted from the method proposed by Chen, et al. [16]. In this experiment, the angular position of the pressure sensor referred to the angle between the position of the pillar structure and the sensing axis of that pressure sensor (Fig. 8). Theoretically, the output voltages at two different angular positions θ_1 and $\theta_1 + \Delta\theta$ should be larger or equal to the noise voltage in order to be distinguishable. The different angle $\Delta\theta$ is then considered to be the angular resolution of the sensor:

$$\Delta V = V_0(\cos(\theta_1 + \Delta\theta) - cos\theta_1) \tag{7}$$

where V_0 is the maximum output voltage of the sensor and ΔV is the noise voltage, which was 0.07 mV, 0.1 mV, 0.08 mV and 0.11 mV in sensor 1, senor 2, sensor 3 and sensor 4 correspondingly. Based on Eq. (7), the angular resolution $\Delta\theta$ depends on the angular position θ_1. Figure 9 illustrated the degrading of the angular sensitivity as the angular position changing from 0° to 90°. In Fig. 9, the maximum angular resolution obtained was 0.33° and the minimum was 9.24°. In another words, the angular sensitivity is high when the flow direction is perpendicular to the sensing axis (or

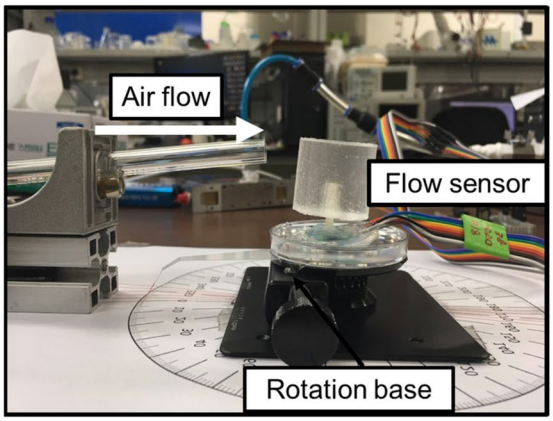

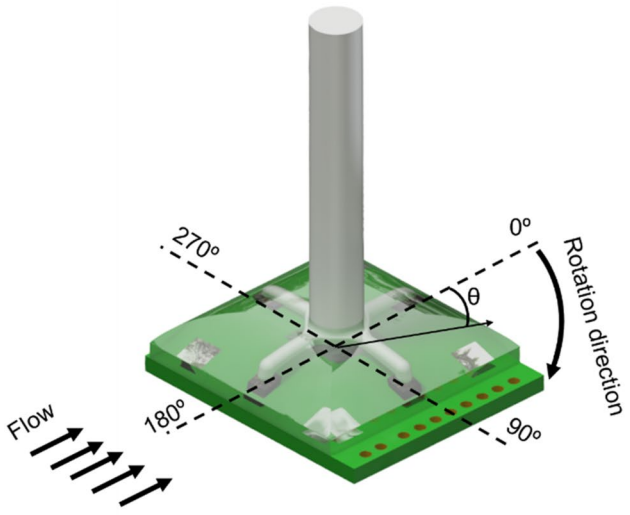

Fig. 8 Setup of the experiment to measure angular resolution

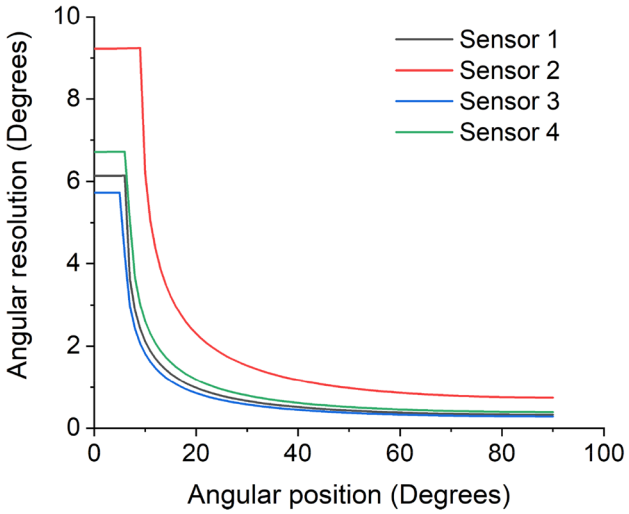

Fig. 9 The angular sensitivity of the as a function of the angular position. The angular position referred to the sensing axis and off axis of each pressure sensor

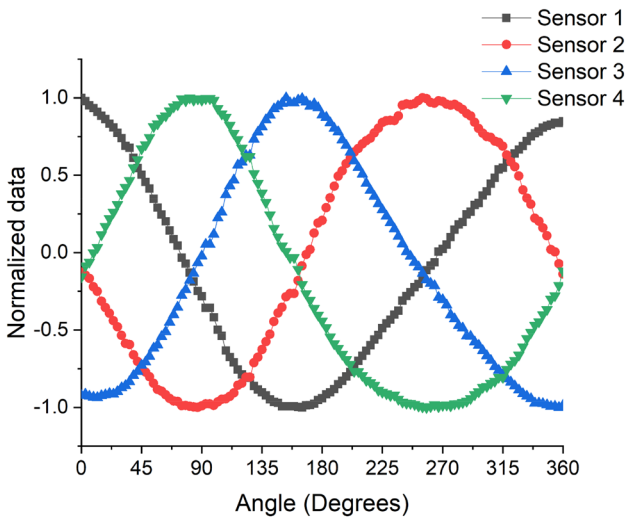

Fig. 10 The normalized output of four pressure sensor in the air. The rotation range was 360° with 3° increasement

parallel to the off axis) and less when the flow direction is parallel to the sensing axis (Fig. 2b). For example, in Fig. 10, sensor 3 signal appeared to have high angular resolution at the angular position of 90° and 270° while less sensitive at the angular position of 0° and 180°.

Additionally, when integrating the four pressure sensors for angular detection, the pressure sensors' outputs compensate each other so that the high angular resolution zone of a sensor can cover the other less sensitive zone. Normalizing pressure sensor output was necessary for the convenience of comparing its output. Figure 10 showed the correlation between four pressure sensor output.

3.4 Discussion and Comparison with Other Flow Sensor Designs

The measured specification of the sensor discussed in this work was compared to a variety of other documented flow sensors in Table 1. Piezoresistive sensors are preferable for flow sensing over piezoelectric sensors because their resistance changes in direct response to material deformation and not the rate of deformation. As a consequence, piezoresistive sensors yield stable outputs even for static stimuli, which is an advantage of piezoresistive sensors over piezoelectric ones. Among previous designs [39, 40], the cantilever (or hair cell) was constructed of piezoresistive materials and exposed to the flow directly. These piezoresistive flow sensors could detect flows of under 20 mm/s, which was suitable for both object detection or location purposes. Thermal transfer flow sensor was less prone to breakage but its low response time (a few seconds) limited their application [31]. The optical flow sensor appeared to have high resolution and sensitivity. However, the complex optical setup makes it unsuitable for AUV application.

In terms of physical dimension, the sensor developed in this work is larger than other piezoresistive-base flow sensors (Table 1). As the goal of this work was to sense low steady DC flow of 5 mm/s, the sensor's size was increased for the sake of resolution and sensitivity, according to Eq. (5). Considering the application of this work, AUVs commonly have maximum dimension ranging from tens to hundreds of centimeters [39, 41]. The size of the flow sensor developed in this work was acceptable for the application of the AUV's steady flow sensor.

The fabrication of the cilia, cover, cupula mold was done using 3D printing technology. The application of 3D printing allows us to rapidly fabricate the prototype from a design in a few hours. In comparison, MEMS sensors require the fabrication to take several weeks minimum, and it is hard to have any modification in the design once fabricated. We chose to use 3D printed parts, because it was easy to make design changes or fix a failed fabrication batch, which was advantageous for making of prototypes [40]. Also, 3D printing can be cost effective for small volumes, whereas MEMS sensors are cost effective in large volumes.

Table 1 A comparison between this work and other state-of-the-art work on flow sensors

Ref.	Operation principle	Size	Performance	Span	Angular resolution	Remarks
[39]	Piezoresistive	Cantilever: 1.5 × 0.1 × 0.6 mm	Sensitivity: 0.07 mV/mm/s	N/A	N/A	Object detecting Sensing DC flow rate
[40]	Piezoresistive	Cantilever: 1.5 × 0.1 × 0.6 mm	90 mm/s error for 500 mm/s in air	N/A	N/A	Linear response Sensing DC flow rate
[44]	Piezoresistive	Cupula: 2.7 × 1 mm	Resolution: 18 mm/s Sensitivity: 77 mV/m/s in water	0–500 m/s	N/A	Cupula structure increase sensitivity 3.5 times Sensing DC flow rate
[45]	Strain gauge base	Cilia: 1.5 × 4 mm Cantilever: 4.5 × 1.5 × 1.5 mm	Resolution: 58 mm/s Sensitivity: 30 mV/m/s	58–90 mm/s	N/A	Sensing AC flow rate
[33]	Piezoelectric	2.7 × 3.5 mm	Sensitivity: 22 mV/mm/s	8.2 μm/s	N/A	Biomimetic CN sensor Sensing AC flow rate
[16]	Piezoresistive	700 μm tall hair cell	Resolution: 0.7 mm/s	N/A	2.16°	Study of the biological world Sensing AC flow rate
[13]	Optical	Pillar length: 64.8 mm Sphere radius: 4 mm	Max. resolution 5 μm/s	N/A	1.8°	Resolution depends on stimulation frequency Sensing AC flow rate
[31]	Thermal	3 × 3 mm chip	Resolution: 500 mm/s	0–10 m/s	5°	High power consumption Sensing DC flow rate
This work	Piezoresistive	Pillar: 3 mm × 20.6 mm Cupula: 30 mm × 30 mm	Resolution: 4.93 mm/s Sensitivity: 20.3 mV/m/s	0–500 m/s	9.24°	Nonlinear Sensing DC flow rate

A disadvantage of our design is the sensor's fragility. As long as the flow sensor is exposed to the environment, it is at risk of being damaged by high reverse flow, turbulence, or collision during maneuvering. The flow sensor discussed in this work was filled and covered with a soft silicone material called Ecoflex™. The purpose was to increase robustness and provide waterproofing for the pressure sensor dies inside. In addition, the flexibility of the cured Ecoflex™ enhances the spring effect, which moves the pillar back to its original position when not exposed to flow forces. One of the concerns raised in this investigation was that sensors filled with Ecoflex™ would have reduced sensitivity. As Ecoflex™ exhibits high nonlinearity [42], it is challenging to include Ecoflex™ into theoretical model. However, as far as we understand, Ecoflex™ acted as a spring that connects between the pillar and pressure sensor. Depending on the targeted detection flow rate, the amount of Ecoflex™ can be tailored to provide enough sensitivity while still provide enough protection to the pressure sensors.

The flow sensor was designed to support AUVs by means of providing necessary flow information for maneuvering. Along with IMU and GPS, the flow sensor increased the operation range of AUVs in harsh marine zones [43]. In addition, as an extension application of this sensor, the flow sensor can be used to monitor flow rate in different environments, such as water treatment plants and sewage systems. It is important to carefully monitor the flow rate in water treatment facilities to ensure a proper purification process as well as high-quality water produced. The potential contribution of the presented flow sensor in environmental researches remains promising though further works are necessary to realize its applications.

4 Conclusion

In this work, a biomimetic flow sensor was developed that was capable of detecting flow rate and direction simultaneously for AUV applications. The design was inspired by the fish neuromast structure. The pillar was designed to be robust and 3D printed with high precision. Pressure sensors were utilized for the sensing element, which allowed high accuracy and sensitivity. The sensor was shown to detect the minimum flow rate of 4.93 mm/s. The angular resolution was 9.24°. The flow sensor is expected to support the maneuvering of AUVs in harsh conditions.

Acknowledgements The authors gratefully acknowledge the Seoul National University of Science and Technology for providing facilities to conduct this research. The authors sincerely appreciate the contribution of Miniaturized Medical Systems Lab, Seoul National University of Science and Technology: Ji-Won Chon, Kwan-Jun Jang, Eung-Cheon Kim, Hyun-Seung Ko to complete the research.

Author Contributions W-TP supervised the findings of this work. L-GT designed and performed the experiment, derived the models and analyzed the data. All authors contributed to the final manuscript.

Funding This work was supported by Grant No. 10060065 from the Industrial Source Technology Development Program of the MOTIE (Ministry Of Trade, Industry and Energy), Korea.

Compliance with Ethical Standards

Conflict of Interest This work has not been published elsewhere and that it has not been submitted simultaneously for publication elsewhere. The authors declare that they have no conflicts of interest.

References

1. G. T. C. Panel. (1984). *Global tropospheric chemistry: a plan for action*. Washington: National Academies Press.
2. Abdullah, A. M., et al. (2018). Review of the control system for an unmanned underwater remotely operated vehicle. In *Engineering applications for new materials and technologies* (pp. 609–631), Springer.
3. Paull, L., Saeedi, S., Seto, M., & Li, H. (2014). AUV navigation and localization: a review. *IEEE Journal of Oceanic Engineering, 39*(1), 131–149.
4. Tran, N.-H., Choi, H.-S., Bae, J.-H., Oh, J.-Y., & Cho, J.-R. (2015). Design, control, and implementation of a new AUV platform with a mass shifter mechanism. *International Journal of Precision Engineering and Manufacturing, 16*(7), 1599–1608.
5. Park, H.-G., Ahn, K.-K., Park, M.-K., & Lee, S.-H. (2018). Study on robust lateral controller for differential GPS-based autonomous vehicles. *International Journal of Precision Engineering and Manufacturing, 19*(3), 367–376.
6. Montgomery, J. C., Baker, C. F., & Carton, A. G. (1997). The lateral line can mediate rheotaxis in fish. *Nature, 389*(6654), 960.
7. Kroese, A. B. A., Van der Zalm, J. M., & Van den Bercken, J. (1978). Frequency response of the lateral-line organ of Xenopus laevis. *Pfluegers Archiv, 375*(2), 167–175.
8. Yoshizawa, M., Jeffery, W. R., van Netten, S. M., & McHenry, M. J. (2014). The sensitivity of lateral line receptors and their role in the behavior of Mexican blind cavefish (*Astyanax mexicanus*). *Journal of Experimental Biology, 217*(6), 886–895.
9. Coombs, S. (2001). Smart skins: information processing by lateral line flow sensors. *Autonomous Robots, 11*(3), 255–261.
10. Montgomery, J., Bleckmann, H., & Coombs, S. (2013). Sensory ecology and neuroethology of the lateral line. In *The lateral line system* (pp. 121–150), Springer.
11. Kanhere, E., Wang, N., Asadnia, M., Kottapalli, A.G.P., & Miao, J.M. (2015). Crocodile inspired Dome Pressure sensor for hydrodynamic sensing. In *Solid-state sensors, actuators and microsystems (TRANSDUCERS), 2015 transducers-2015 18th international conference on* (pp. 1199–1202).
12. Dusek, J.E. (2016). Development of bio-inspired distributed pressure sensor arrays for hydrodynamic sensing applications. Massachusetts Institute of Technology.
13. Wolf, B. J., Morton, J. A. S., MacPherson, W. B. N., & van Netten, S. M. (2018). Bio-inspired all-optical artificial neuromast for 2D flow sensing. *Bioinspiration & Biomimetics*, *13*(2), 026013.
14. Klein, A., & Bleckmann, H. (2011). Determination of object position, vortex shedding frequency and flow velocity using artificial lateral line canals. *Beilstein Journal of Nanotechnology, 2,* 276.

15. Lee, H. S., et al. (2014). Flexible inorganic piezoelectric acoustic nanosensors for biomimetic artificial hair cells. *Advanced Functional Materials, 24*(44), 6914–6921.
16. Chen, N., Tucker, C., Engel, J. M., Yang, Y., Pandya, S., & Liu, C. (2007). Design and characterization of artificial haircell sensor for flow sensing with ultrahigh velocity and angular sensitivity. *Journal of Microelectromechanical Systems, 16*(5), 999–1014.
17. Hu, X., Jiang, Y., Ma, Z., Xu, Y., & Zhang, D. (2019). Bio-inspired flexible lateral line sensor based on P(VDF-TrFE)/BTO nanofiber mat for hydrodynamic perception. *Sensors*, *19*(24), 5384.
18. Yang, Y., et al. (2006). Distant touch hydrodynamic imaging with an artificial lateral line. *Proceedings of the National Academy of Sciences, 103*(50), 18891–18895.
19. Lee, J., Kim, T. G., Kim, D., Kim, J., & Lim, S.-H. (2017). Improvements in the performance of a microthermal flow sensor using asymmetrically located temperature sensors. *International Journal of Precision Engineering and Manufacturing, 18*(2), 227–231.
20. Bian, Y., Zhang, Y., & Xia, X. (2016). Design and fabrication of a multi-electrode metal-core piezoelectric fiber and its application as an airflow sensor. *Journal of Bionic Engineering, 13*(3), 416–425.
21. Droogendijk, H., Bruinink, C. M., Sanders, R. G. P., Dagamseh, A. M. K., Wiegerink, R. J., & Krijnen, G. J. M. (2012). Improving the performance of biomimetic hair-flow sensors by electrostatic spring softening. *Journal of Micromechanics Microengineering, 22*(6), 65026.
22. Tran, L., Joo, D., & Park, W. (2019). A bioinspired piezoelectric cilia array for sensing of hydrodynamic flow. In *2019 20th International conference on solid-state sensors, actuators and microsystems & eurosensors XXXIII (TRANSDUCERS & EUROSENSORS XXXIII)* (pp. 1937–1940).
23. Herzog, H., Steltenkamp, S., Klein, A., Tätzner, S., Schulze, E., & Bleckmann, H. (2015). Micro-machined flow sensors mimicking lateral line canal neuromasts. *Micromachines, 6*(8), 1189–1212.
24. Herzog, H., et al. (2015). μ-Biomimetic flow-sensors—introducing light-guiding PDMS structures into MEMS. *Bioinspiration & Biomimetrics, 10*(3), 36001.
25. Ejeian, F., et al. (2019). Design and applications of MEMS flow sensors: a review. *Sensors and Actuators A: Physical, 295,* 483–502.
26. Fan, Z., Chen, J., Zou, J., Bullen, D., Liu, C., & Delcomyn, F. (2002). Design and fabrication of artificial lateral line flow sensors. *Journal of Micromechanics Microengineering, 12*(5), 655.
27. Ko, H., et al. (2015). Bioinspired piezoresistive acceleration sensor using artificial filiform sensillum structure. *Sensors and Materials, 27*(6), 437–445.
28. Han, Z., et al. (2018). Artificial hair-like sensors inspired from nature: a review. *Journal of Bionic Engineering, 15*(3), 409–434.
29. Ozaki, Y., Ohyama, T., Yasuda, T. & Shimoyama, I. (2000). An air flow sensor modeled on wind receptor hairs of insects. In *Micro electro mechanical systems, 2000. MEMS 2000. The thirteenth annual international conference on* (pp. 531–536).
30. Ma, R.-H., Chou, P.-C., Wang, Y.-H., Hsueh, T.-H., Fu, L.-M., & Lee, C.-Y. (2009). A microcantilever-based gas flow sensor for flow rate and direction detection. *Microsystem Technologies, 15*(8), 1201–1205.
31. Kim, S., Nam, T., & Park, S. (2004). Measurement of flow direction and velocity using a micromachined flow sensor. *Sensors and Actuators A: Physical, 114*(2), 312–318.
32. Xu, Y., & Mohseni, K. (2017). A pressure sensory system inspired by the fish lateral line: hydrodynamic force estimation and wall detection. *IEEE Journal of Oceanic Engineering, 42*(3), 532–543.
33. Asadnia, M., Kottapalli, A. G. P., Miao, J., Warkiani, M. E., & Triantafyllou, M. S. (2015). Artificial fish skin of self-powered micro-electromechanical systems hair cells for sensing hydrodynamic flow phenomena. *Journal of the Royal Society, Interface, 12*(111), 20150322.
34. Abdulsadda, A. T., & Tan, X. (2013). Underwater tracking of a moving dipole source using an artificial lateral line: algorithm and experimental validation with ionic polymer–metal composite flow sensors. *Smart Materials and Structures, 22*(4), 45010.
35. Haehnel-Taguchi, M., Akanyeti, O., & Liao, J. C. (2014). Afferent and motoneuron activity in response to single neuromast stimulation in the posterior lateral line of larval zebrafish. *Journal of Neurophysiology, 112*(6), 1329–1339.
36. Fay, R.R., & Simmons, A.M. (1999). The sense of hearing in fishes and amphibians. In *Comparative hearing: fish and amphibians* (pp. 269–318), Springer.
37. Van Trump, W. J., & McHenry, M. J. (2008). The morphology and mechanical sensitivity of lateral line receptors in zebrafish larvae (Danio rerio). *Journal of Experimental Biology, 211*(13), 2105–2115.
38. Raffel, M., Willert, C. E., Scarano, F., Kähler, C. J., Wereley, S. T., & Kompenhans, J. (2018). *Particle image velocimetry: a practical guide*. Berlin: Springer.
39. Qualtieri, A., Rizzi, F., Todaro, M. T., Passaseo, A., Cingolani, R., & De Vittorio, M. (2011). Stress-driven AlN cantilever-based flow sensor for fish lateral line system. *Microelectronic Engineering, 88*(8), 2376–2378.
40. Abels, C., Qualtieri, A., De Vittorio, M., Megill, W. M., & Rizzi, F. (2016). A bio-inspired real-time capable artificial lateral line system for freestream flow measurements. *Bioinspiration & Biomimetrics, 11*(3), 35006.
41. Jeong, S.-K., et al. (2016). Design and control of high speed unmanned underwater glider. *International Journal of Precision Engineering and Manufacturing-Green Technology, 3*(3), 273–279.
42. Steck, D., Qu, J., Kordmahale, S. B., Tscharnuter, D., Muliana, A., & Kameoka, J. (2019). Mechanical responses of Ecoflex silicone rubber: compressible and incompressible behaviors. *Journal of Applied Polymer Science, 136*(5), 47025.
43. Wynn, R. B., et al. (2014). Autonomous Underwater Vehicles (AUVs): their past, present and future contributions to the advancement of marine geoscience. *Marine Geology, 352,* 451–468.
44. Kottapalli, A. G. P., Bora, M., Asadnia, M., Miao, J., Venkatraman, S. S., & Triantafyllou, M. (2016). Nanofibril scaffold assisted MEMS artificial hydrogel neuromasts for enhanced sensitivity flow sensing. *Scientific Reports, 6,* 19336.
45. Kamat, A. M., Pei, Y., & Kottapalli, A. G. P. (2019). Bioinspired cilia sensors with graphene sensing elements fabricated using 3D printing and casting. *Nanomaterials, 9*(7), 954.

Le-Giang Tran received his B.S. degree in Biomedical Engineering from HCMC International University, Vietnam in 2014 and M.S. degree in Biomedical Engineering and Biomaterials from Seoul National University of Science and Technology in 2016. For his M.S. research, he worked on developing a wireless power transfer system for biomedical applications. He is currently pursuing Ph.D. degree in Seoul National University of Science and Technology and is focusing on flow sensor for unmanned underwater vehicles and microneedles for intradermal drug delivery.

Woo-Tae Park received the B.S. degree in mechanical design from Sungkyunkwan University, Korea, in 2000, the M.S. and Ph.D. degrees in mechanical engineering from Stanford University in 2002 and 2006 respectively. For his Ph.D., he worked on wafer scale encapsulated MEMS devices for biomedical applications. After graduation, he worked at Intel Corporation, Freescale Semiconductor, and IME Singapore, leading several projects on MEMS development. He has authored more than 80 journals and refereed conference papers and has 14 issued and pending patents. He is currently an associate professor at Seoul National University of Science and Technology, conducting research on microscale medical devices.